AGU ADVANCING EARTH AND SPACE SCIENCE

Geophysical Research Letters

RESEARCH LETTER
10.1029/2021GL093292

Drivers of Subseasonal Forecast Errors of the East African Short Rains

E. W. Kolstad[1,2], D. MacLeod[3], and T. D. Demissie[1,4]

[1]NORCE Norwegian Research Center, Bjerknes Center for Climate Research, Bergen, Norway, [2]Norwegian Meteorological Institute, Bergen, Norway, [3]School of Geographical Sciences, University of Bristol, Bristol, UK, [4]CGIAR Research Program on Climate Change, Agriculture and Food Security (CCAFS) East Africa, Addis Ababa, Ethiopia

Key Points:

- Subseasonal forecast errors of the East African 'short rains' at 3–4 weeks' lead time are studied for the European Center for Medium-Range Weather Forecasts monthly forecasting system
- The rainfall errors are linked to the initial state of the Indian Ocean dipole through forecast errors of oceanic and atmospheric drivers
- Knowledge about these conditional errors can be used for a priori forecast correction and to inform targeted model improvements

Correspondence to:
E. W. Kolstad,
ekol@norceresearch.no

Citation:
Kolstad, E. W., MacLeod, D., & Demissie, T. D. (2021). Drivers of subseasonal forecast errors of the East African short rains. *Geophysical Research Letters*, *48*, e2021GL093292. https://doi.org/10.1029/2021GL093292

Received 10 MAR 2021
Accepted 23 JUN 2021

Abstract The 'short rains' in East Africa from October to December have significant year-to-year variability. Their abundance or deficiency is often associated with floods or droughts for which early warning is crucial, though even in normal seasons skillful forecasts facilitate planning and preparedness. Here we study the relationship between initial-state sea surface temperatures and subseasonal rainfall forecast errors in the European Center for Medium-Range Weather Forecasts model in the region. We demonstrate that the initial mode of the Indian Ocean Dipole (IOD) is a partial control on the rainfall error in weeks 3–4. This relationship is also clear on the seasonal scale, exemplified by too-wet forecasts during the 2015 season when the IOD was positive, and too-dry forecasts in 2010 when it was negative. Our results provide an entry point for model improvement, and we show that *a priori* forecast corrections based on the initial IOD index are feasible.

Plain Language Summary In East Africa, the rainfall is usually concentrated in specific periods of the year. One of these periods occurs between October and December and is called the 'short rains'. Failure of the short rains can have disastrous effects on farmers and pastoralists, as there exist little infrastructure for irrigation in the region. Similarly, too heavy rains can yield devastating floods. Advance knowledge of the timing and nature of the short rains is therefore crucial for planning and preparedness. However, the usefulness of any prior information is contingent on accurate forecasts, which are mainly based on numerical models. Here we study the ability of a widely used such model, focusing on whether it is possible to predict the model error already when the forecasts are issued. We find that the sea surface temperatures in the nearby Indian Ocean influence the development of rainfall errors in the model. This information can be used to guide *upfront* forecast correction, but it also offers a diagnosis that can inform model improvements. Both actions have the potential to enhance the quality of East African rainfall forecasts.

1. Introduction

Floods and droughts have significant impacts on lives and livelihoods in East Africa (e.g., Conway et al., 2005; Haile et al., 2019; Little et al., 2001). The short rains from October to December (OND) show substantial interannual variability and extreme impacts from both flooding (e.g., in 2019; Wainwright et al., 2021) and drought (e.g., in 2010; Robinson et al., 2019). Numerous studies have demonstrated skill in predicting the short rains at seasonal scales (Hastenrath et al., 2004; MacLeod, 2018; Mwangi et al., 2014; Ogutu et al., 2017; Philippon et al., 2002; Young & Klingaman, 2020). Most of the skill arises from links between rainfall and sea-surface temperature (SST) anomalies over the eastern Pacific (the El Niño–Southern Oscillation; ENSO), as well as Indian Ocean SST and wind anomalies (Behera et al., 2005; Black, 2005; Funk et al., 2018; Hastenrath, 2007; Indeje et al., 2000; Liu et al., 2020; Mutai & Ward, 2000; Mutai et al., 1998; Ummenhofer et al., 2009; Zhao & Cook, 2021).

Seasonal and subseasonal forecasts can play complementary roles in planning and preparedness (e.g., Bruno Soares et al., 2018; Bazo et al., 2019; Lemos et al., 2012; Nyamekye et al., 2021; Tall et al., 2018), with seasonal forecasts triggering preparedness several months ahead of a season, and subseasonal forecasts allowing targeted interventions within the season. Although seasonal forecasts have been provided at the Greater Horn of Africa Regional Climate Outlook Forums (GHACOF) for over a decade (Hansen et al., 2011; Walker et al., 2019), subseasonal forecasts that indicate potential anomalies over the upcoming few weeks are not

routinely disseminated in East Africa. This means that following the pre-season outlook, the next rainfall forecast update is often issued only a few days ahead of the hazard (e.g., Kilavi et al., 2018), limiting the potential for risk management.

The lack of subseasonal forecast provision is unfortunate, as compared to most of the globe East Africa is a hotspot of forecast skill (de Andrade et al., 2020; Vigaud et al., 2019). The strong predictability arises in large part from the Madden-Julian Oscillation (MJO), which shows a strong teleconnection with regional rainfall: models with skillful MJO predictions also capture the teleconnection to rainfall over East Africa (MacLeod et al., 2021).

An impediment to the uptake of subseasonal forecasts is a lack of robust understanding of model performance in the region. Recent studies are addressing parts of this knowledge gap by demonstrating levels of model skill and evaluating model representation of teleconnections (Hirons & Turner, 2018; King et al., 2021; Walker et al., 2019). However, most studies focus on unconditional model errors (e.g., mean model biases) rather than conditional model errors, that is, forecast errors associated with particular climate states (e.g., Kolstad et al., 2020; Matsueda & Palmer, 2018; Minami & Takaya, 2020). Understanding of conditional model errors can give two benefits supporting the reliability of operational forecasts. First, it can make possible a context-specific *a priori* error correction: knowing that the model will behave a certain way under a certain climate state allows a more intelligent use of model output. Second, it provides targeted error feedback to model developers, which can potentially lead to improvement of simulation realism in the region and higher model skill.

Here, we study the conditional model error of subseasonal forecasts of the East African short rains. In particular, we investigate the relationship between the initial state of the Indian Ocean Dipole (IOD; Marchant et al., 2007) and subsequent forecast error developments. Our aim is to enhance understanding of model performance, which we hope may contribute to raising the level of trust in forecasts on decision-relevant time scales.

2. Data and Methods

2.1. Data

The European Center for Medium-Range Weather Forecasts (ECMWF) monthly forecasts are issued twice a week. The model version used here is CY46R1, which has a native horizontal atmospheric grid spacing after day 15 of about 32 km, and the ocean model is NEMO3.4.1, with a native 0.25° grid spacing. Although the 32 km grid spacing is insufficient for resolving small-scale convective systems, it is sufficient for reproducing the large-scale rainfall characteristics driven by ENSO and the Walker Circulation over the Indian Ocean. A set of 11-member hindcasts is produced for each forecast, initialized for the same day and month of the previous 20 years. From the S2S database (Vitart et al., 2017), we use the ensemble means of the first 11 members of the (51-member) forecasts for which all lead times between 15 and 28 days (3–4 weeks) occurred between October 1 and December 31, 2019, as well as their associated hindcasts. This comprises $23 \times 21 = 483$ model runs. The variables studied are precipitation (hereafter referred to as "rainfall"), zonal wind at 850 and 200 hPa, and SST, all interpolated to 1.5° grids, which is how the atmospheric data are stored in the S2S database. For the same two-week periods, we also calculate accumulated rainfall from the Climate hazards infrared precipitation with stations (CHIRPS) data set (Funk et al., 2015), interpolated to the 1.5° model grid. For the other variables, we use ERA5 reanalysis data (Hersbach et al., 2018a; 2018b; 2020) as our reference.

2.2. Standardization

To account for spatial heterogeneity and model bias, we post-process the rainfall data in several steps. First, we standardize the 483 rainfall time series for each grid point from both the forecasts and the CHIRPS data by subtracting the datewise climatological mean and dividing by the datewise interannual standard deviation. The smooth the climatologies, they are based on data from all (171, on average) dates up to 14 ordinal days before or after the ordinal day of the reference date. Second, we calculate the area-average of the standardized forecast anomalies within our focus region – between 30°E and 52°E and between 10°S

and 12°N (see Figure 1a), following Vigaud et al. (2019) – as $F = \sum w_i f_i$, where F stands for "Forecast", the sum is performed for all land points, the weight of each grid point value is $w_i = \cos \varphi_i \,/\, \sum \cos \varphi_j$, where φ_i is the latitude of land point i and the sum is performed for all land points, and f_i is the standardized forecast anomaly in i. Similarly, we calculate the area-averaged CHIRPS rainfall anomalies as $O = \sum w_i o_i$ (O for "Observations"). Third, we define the forecast error as $\varepsilon = F - O$. Note that ε is identical to the area-average of the forecast error in each grid point, as $\varepsilon = \sum w_i \left(f_i - o_i\right) = \sum w_i f_i - \sum w_i o_i = F - O$.

2.3. SST Indices

SST data from ERA5 are used to calculate an IOD index (I henceforth) in two steps. First, we compute area-averaged standardized SST anomalies (using the same climatological smoothing as for the rainfall data) in the western (50°E to 70°E and 10°S to 10°N) and eastern (90°E to 110°E and 10°S to 0°) parts of the Indian Ocean. Second, we take the difference between the western and eastern time series, and third, we standardize the resulting time series. Although our main focus is on the IOD index, we also calculate a NINO3.4 index as area-averaged standardized SST anomalies between 170°W and 120°W and between 5°S and 5°N. The boundaries of the SST regions are shown in Figure 2a.

2.4. Significance Testing

To account for intraseasonal autocorrelation, we use bootstrapping to create sets of 1,000 artificial time series to contrast with the actual time series. Each time series consists of data from 23 initial dates per year, and in the artificial time series, we replace each set of 23 elements with a set from a random year between 1999 and 2019 (with replacement). This retains the intraseasonal autocorrelation. The null hypothesis that actual correlation or regression coefficients could just as well have resulted from the randomized, artificial sets can be rejected at the 5% significance level (which is used throughout) if the actual coefficient falls outside the interval between the 2.5th and 97.5th percentiles of the artificial set.

2.5. Linear Prediction Model

In Section 3.2, we use a linear regression model to predict O based on the predictors F and I:

$$O = a_F \times F + a_I \times I + \epsilon. \tag{1}$$

The coefficients are estimated (by minimizing the residual ϵ using ordinary least squares) for each forecast time by using F and I for all the other forecast times ("leave-one-out" cross validation), and we call the best estimates $\hat{a}_F$ and $\hat{a}_I$, so that the prediction of O can be written as:

$$\hat{O} = \hat{a}_F \times F + \hat{a}_I \times I. \tag{2}$$

Note that we do not compute out-of-sample climatologies for each element of the time series, as the high number of data points these are based on (171, on average) makes the in-sample effect negligible.

3. Results

3.1. The Short Rains

We first present an overview of the short rains' relative importance in the annual rainfall cycle, as well as its representation by the model. The ratios in Figure 1a were obtained by dividing the average rainfall during all the 483 OND forecast periods by the average rainfall during all similar periods throughout the year. The OND rainy season is most dominant compared to the rest of the year in Somalia, southern Ethiopia, and eastern Kenya, but ratios above 1 also occur in other parts of the study region, including its southwestern part.

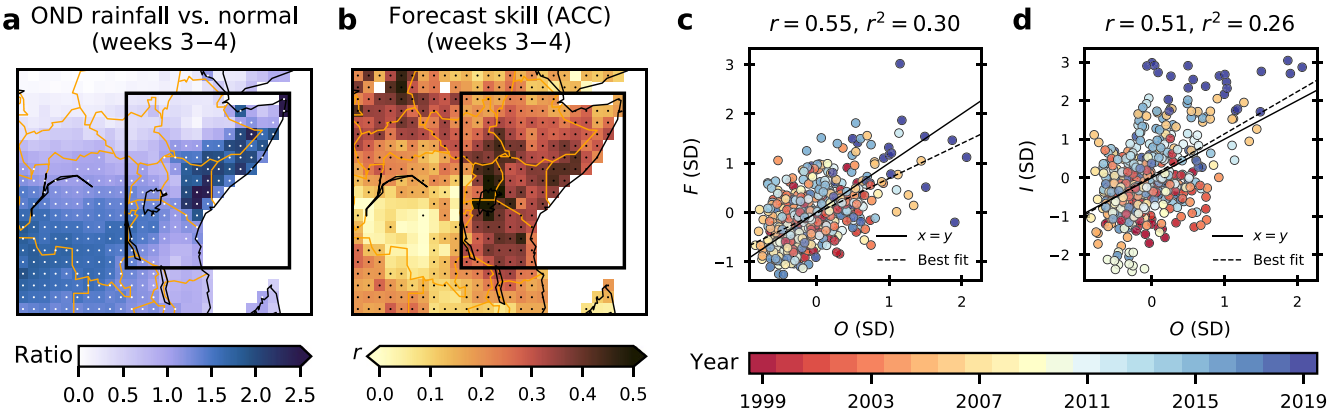

Figure 1. (a) Ratio of October to December rainfall to normal rainfall, with white dots indicating ratios above 1 and the black rectangle showing the boundaries of the focus region. Country borders are shown in orange. (b) Anomaly correlation between the ECMWF forecasts and CHIRPS rainfall, averaged for 3–4 weeks of lead time. Significant coefficients are indicated with dots. (c) Scatter plot of O on the x-axis versus F on the y-axis. The unit is standard deviations (SD), the identity line is solid, and the dashed line shows the best linear fit. The colors are unique for each year, as indicated by the legend below. (d) As (c), but for I instead of F on the y-axis.

Figure 1b shows that the anomaly correlation between the forecasts and the regridded CHIRPS rainfall is significant in most of the whole study region. The minimum, maximum and median correlation coefficients within the region are −0.01, 0.61, and 0.31, respectively. On the spatially aggregated scale, the (significant) correlation between F and O is 0.55 (Figure 1c). This is substantially higher than the median of the grid point correlations, and it means that the ensemble mean forecast explains 30% of the rainfall variability 3–4 weeks in advance on the aggregated scale. The best fit line is less steep than the identity line (i.e., where $x = y$), indicating that F needs calibration. Figure 1d shows a scatter plot of I versus O. The correlation is 0.51, which is lower than the correlation between F and O. In 2019, the high I values are associated with a wide range of O values from about zero to the five largest values in the study period. There is clearly information in I not captured by F, suggesting that a prediction model based on combining F and I might be worthwhile to test (see Section 3.2).

Although not shown, we note here that the correlation between O and the initial NINO3.4 index is only 0.23. As a result, our focus hereafter is on the IOD index.

3.2. Linking Initial SSTs and Rainfall Forecast Errors

While it is well-known that East African OND rainfall is correlated with both ENSO and the IOD, Figure 2a demonstrates that the forecast error ε is also lag-correlated with initial tropical SSTs. This means that the ECMWF model has a systematic bias conditional on the initial state, and it also suggests that initial SSTs can potentially be used to correct the model forecasts *a priori*.

To test whether the forecasts can be corrected based on I, we assess the performance of $\hat{O}$, the linear prediction of O based on F and I (see Section 2.5). A scatter plot O versus $\hat{O}$ is shown in Figure 2b. The correlation between O and $\hat{O}$ is 0.58, which is significantly higher than the correlation between O and F (0.55; see Figure 1c) according to a bootstrapping test (Section 2.4). This means that including I as a predictor in combination with F is indeed worthwhile.

As the correlation between I and ε is relatively high (0.24) and significant (see also Figure 2a), we were curious about why $\hat{O}$ does not represent an even larger improvement with respect to F. It could be related to nonlinear aspects of the relationship between ε and I. Figure 2c shows boxplots (e.g., Krzywinski & Altman, 2014) of ε for four bins organized by ascending I values (the leftmost bin is based on the forecasts initialized when I was in its lower quartile, and so on). The linear part of the relationship between I and ε is reflected by the increasing median values from left to right, but it is also clear that the variance of ε within each bin is large (as each boxplot spans a large range of negative and positive values), and more important: the variance of ε is larger for positive than negative I values. This suggests that a linear model might be unable to capture the whole gamut of the complex and nonlinear relationships between O, F, and I.

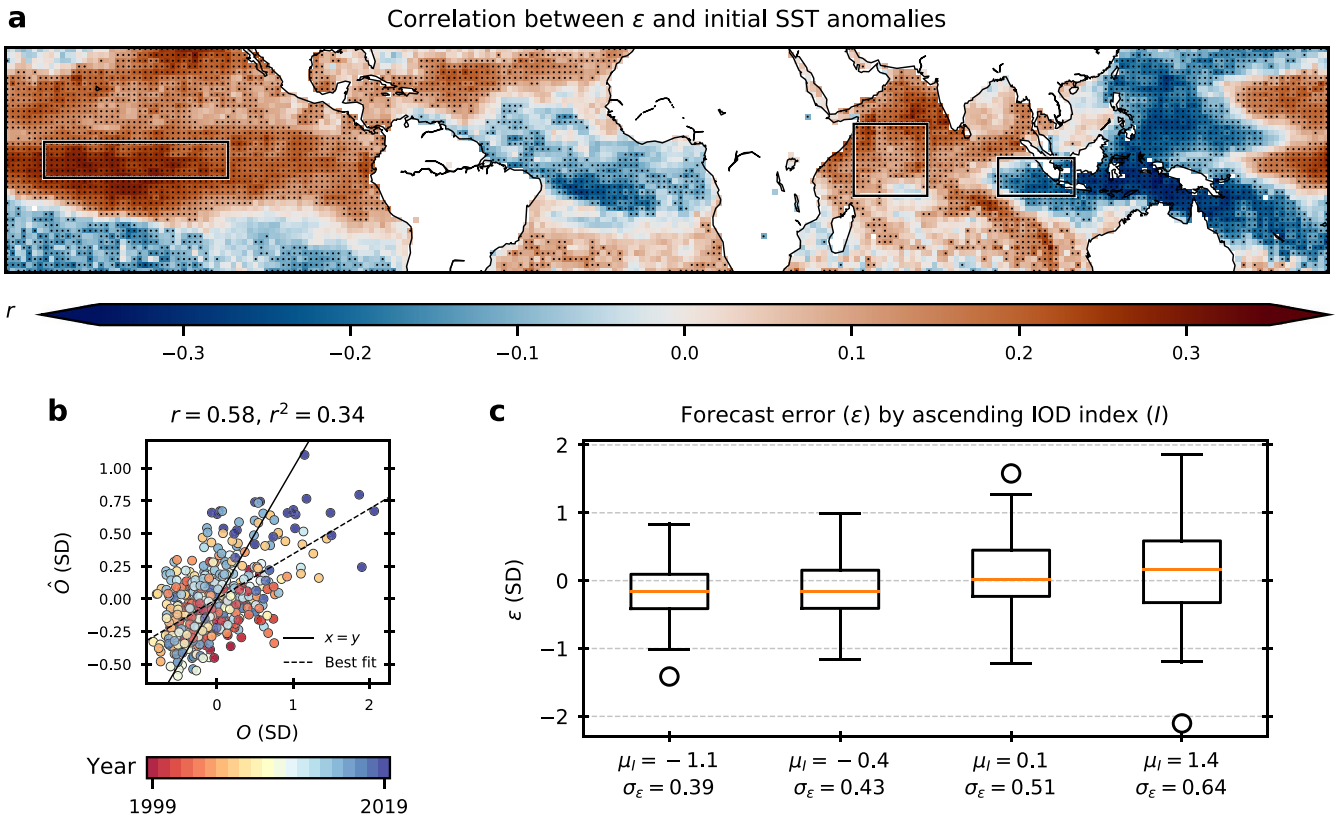

Figure 2. (a) Correlation between inital sea-surface temperature anomalies and ε, with significant values marked with dots. The rectangles indicate the regions used to calculate the NINO3.4 and Indian Ocean Dipole indices. (b) O (x-axis) versus $\hat{O}$ (y-axis), following the scheme in Figures 1c and 1d. (c) Boxplots for four bins arranged from left to right by increasing I values, with the distribution of ε along the y-axis (see text for details). The standard deviation of ε in each bin is printed below the x-axis, along with the mean value of I.

We also tried including the initial NINO3.4 index as a predictor of O, alongside F and I, but its regression coefficient was nonsignificant. This is commensurate with the low correlation between O and the NINO3.4 index (Section 3.1).

3.3. Drivers of Rainfall Forecast Errors

To better understand the dynamics behind the rainfall forecast errors, we show in Figure 3a the correlation between ε and concurrent SST forecast errors. The significant, positive correlations in the northern part of the Indian Ocean demonstrate that the forecast SSTs there are too warm when the model predicts too much rainfall in East Africa ($\varepsilon > 0$) and too cold when the rainfall forecasts are too dry ($\varepsilon < 0$).

Figure 3b reveals significant negative correlations between ε and zonal wind forecast errors at 850 hPa over the ocean and positive correlations over land. Each of these influences is consistent with too-strong low-level convergence over East Africa when $\varepsilon > 0$ and too-weak convergence when $\varepsilon < 0$. Figure 3c shows negative correlations between zonal wind errors at 200 hPa over the continent and off the East African coast, and positive correlations over the eastern Indian ocean. This is an indicator of a surplus of divergence aloft in the western part of the Indian Ocean, which is linked to too strong (weak) convection below 200 hPa in the model when ε is positive (negative).

We now investigate the relationship between I and the SST and zonal wind forecast errors by comparing the correlations shown in the bottom row of Figure 3 with the correlations in the top row. We emphasize that ε does not enter into the calculations of the correlations in the bottom row. Still, the correlation between the SST errors and I (Figure 3d) in the northern Indian Ocean agrees well with the correlations between the same SST errors and ε (Figure 3a). For 850-hPa zonal wind, shown in Figure 3e, there is also good

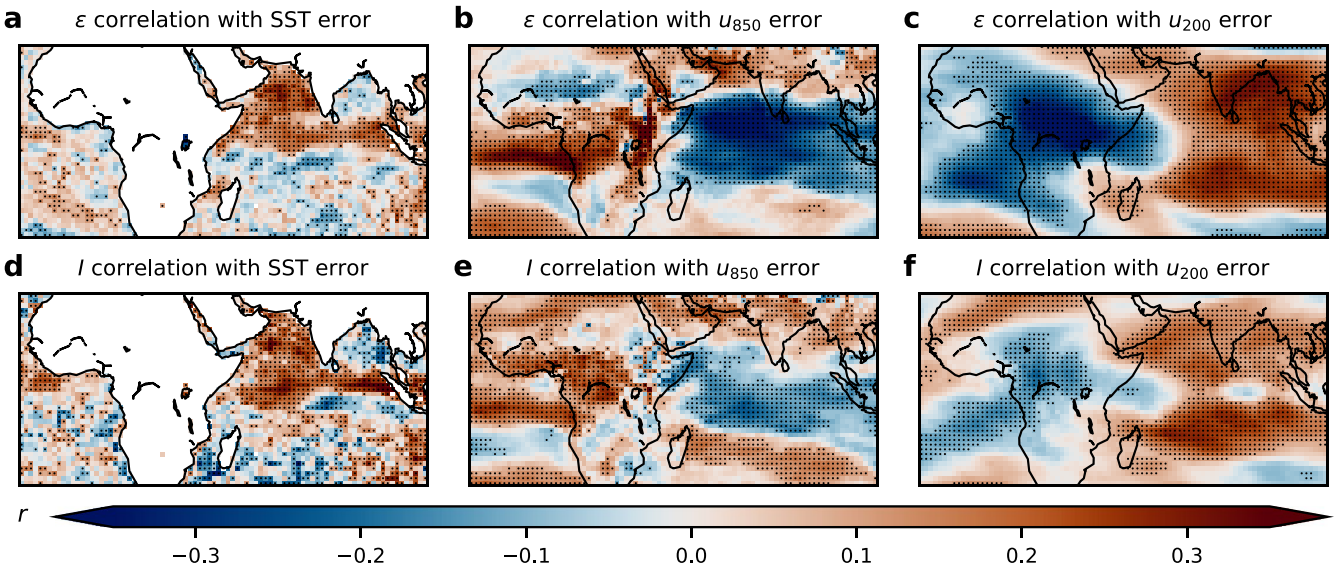

Figure 3. Top row: Correlation between ε and concurrent forecast errors of sea-surface temperature (SST) (a), zonal wind at 850 hPa (b), and zonal wind at 200 hPa (c). Bottom row: Correlation between I and the forecast errors at lead times of 3–4 weeks of SST (d), zonal wind at 850 hPa (e), and zonal wind at 200 hPa (f). Significant coefficients are indicated with dots.

correspondence with Figure 3b over the Indian Ocean, where the correlations are both negative, as well as into the continent from the west, where they are positive. However, the strong north–south oriented positive correlations over the western part of East Africa found in Figure 3b are not replicated in Figure 3e. Similarly, although the correlation of the 200-hPa zonal wind error with both ε (Figure 3c) and I (Figure 3f) is strong over the Indian Ocean, the magnitude of the negative correlation with ε over land is not reproduced for I aloft. This indicates that model errors in representing the variability of the convergence and divergence over the African continent are a determinant of subseasonal forecast errors over East Africa, and that the origin of these errors is only weakly related to the initial state of the IOD.

3.4. Seasonal Means

The aforementioned intraseasonal autocorrelation of forecast errors (e.g., Figure 1c), in combination with a significant link between the initial IOD index and ε, suggest a possibility for *a priori* correction of subseasonal forecast error at the start of the season (or even before, given skillful long-lead SST forecasts). Although based on only 21 seasons, the correlation between the seasonal means of ε and I, shown in Figure 4a, is 0.54 and significant. The seasons with the largest mean ε values on both ends of the scale, 2015 and 2016, also have large I anomalies that match the sign of the mean of ε. Furthermore, the years with the largest positive and negative I values, 2019 and 2010, respectively, also have relatively large mean ε anomalies with matching sign. For these two years the corresponding seasonal mean SST and zonal wind errors are shown in the maps in Figure 4. The spatial patterns are consistent with the correlations in Figure 3, with the high IOD year of 2019 exhibiting positive SST errors in the Indian Ocean (Figure 4b), negative and positive 850-hPa zonal wind errors over the Indian Ocean and Congo basin, respectively (Figure 4c), and positive and negative 200-hPa zonal wind errors over the Indian Ocean and over the continent, respectively (Figure 4d). Qualitatively speaking, similar responses with opposite signs occur in the lowest IOD year of 2010 (Figures 4e–4g).

4. Summary and Discussion

We have demonstrated a robust link between subseasonal rainfall forecast errors over East Africa, tropical SSTs, and the atmospheric circulation. A symmetry has been identified, where positive (negative) IOD states in the initial conditions are associated with too-strong positive (negative) rainfall anomalies over East Africa in the model after 3–4 weeks.

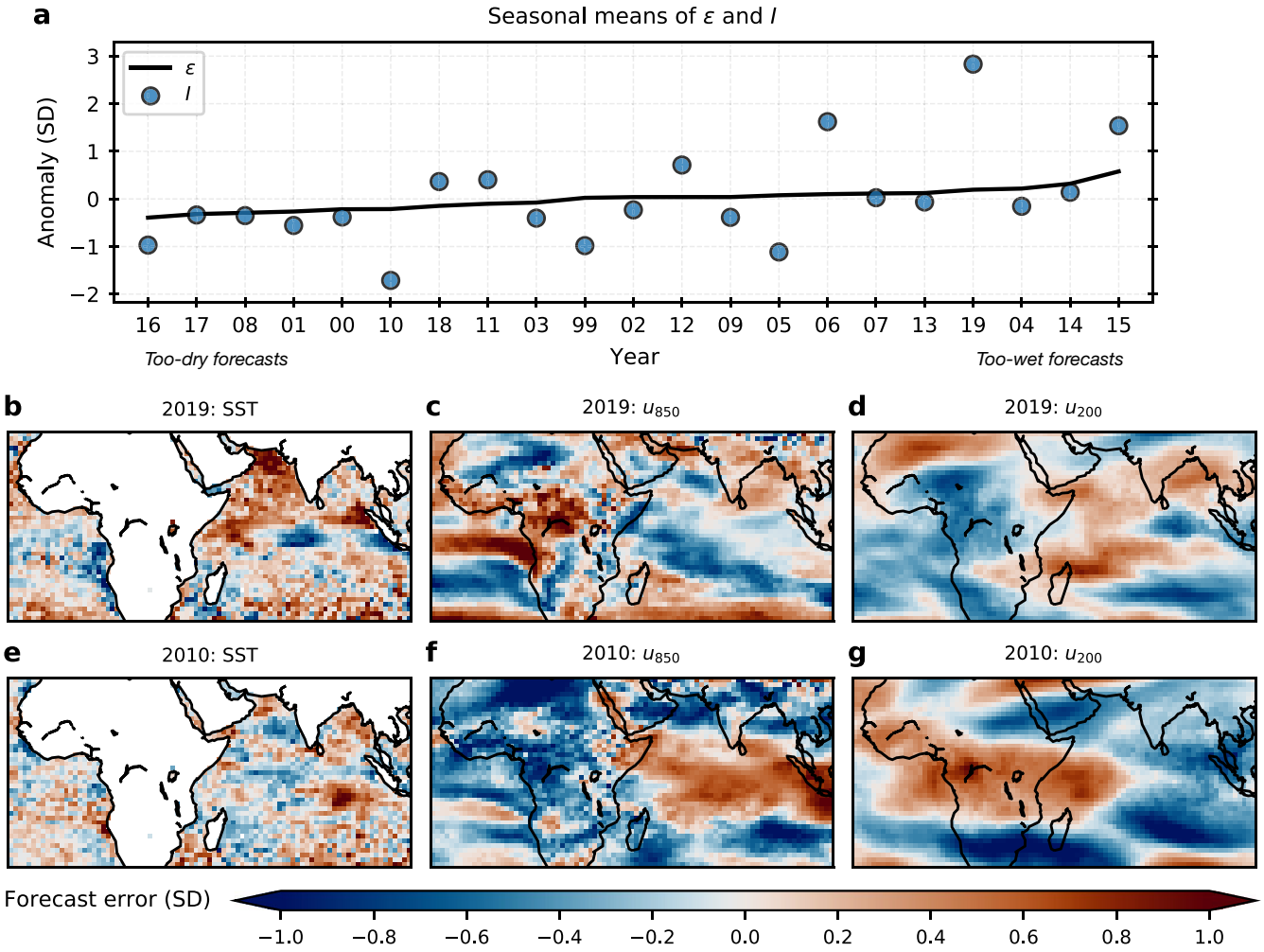

Figure 4. (a) Seasonal means of ε (black line) and I (blue circles), sorted from left to right by ascending ε values. The remaining panels show the seasonal mean standardized forecast errors of sea-surface temperature, zonal wind at 850 hPa, and zonal wind at 200 hPa, in 2019 (b–d) and 2010 (e–g).

A linear correlation approach was used to link the rainfall forecast errors to forecast errors of oceanic and atmospheric drivers (see Figure 3, top row). Focusing on the too-wet forecasts (the too-dry forecasts mainly show "opposite" behavior), these were found to be associated with concurrent model errors in the western Indian Ocean region, specifically in the form of positive SST errors, coupled with too strong divergence aloft and too strong easterly zonal wind anomalies at low levels. Furthermore, we found that the too-wet forecasts are associated with positive low-level zonal wind errors stretching into East Africa from the west. Previous studies have repeatedly demonstrated an association between easterlies over the Indian Ocean and enhanced rainfall and flooding in East Africa (Black et al., 2003; Hastenrath, 2007; Nicholson, 2017). However, the results presented here are unique by linking this state not to rainfall totals, but to errors in the rainfall forecast.

Another key finding is that the correlations between the errors in the forecasts of SSTs and zonal winds and the rainfall forecast error exhibit many similarities to the correlations between the initial IOD index and same variables' forecast errors (Figure 3, bottom row). This suggests oceanic and atmospheric pathways linking the initial IOD index with subsequent rainfall forecast errors. The forecast errors during the two OND seasons with the highest (in 2019) and lowest (in 2010) mean IOD index in the study period confirmed a linkage between the IOD index, rainfall forecast errors and forecast errors of SSTs and zonal winds on the seasonal scale.

These results have two important consequences. The first is that they suggest an opportunity to make a state-dependent correction to the forecasts. This could be done in a systematic way whereby forecasts initialized in anomalous SST states are calibrated, with a correction to the ensemble mean rainfall forecast. As a proof-of-concept exercise, this was done here with a linear adjustment of the forecast based on the initial IOD index in Section 3.2, and the corrected forecast had significantly higher skill than the uncorrected forecast. We emphasize that our intention is to demonstrate the potential for using initial SSTs to create a hybrid empirical/dynamical forecast model, and not to optimize such a model. Thus, we did not attempt to correct the rainfall forecasts on the local scale (see skill in Figure 1b), but the promising results for the aggregated geographical scale suggest that it might be possible. But even without a systematic calibration, knowledge of the systematic relationship between initial SSTs and rainfall forecast errors is likely to be useful to experienced forecasters, who may incorporate this into their subjective interpretation when developing forecast products.

The second main consequence is that our results provide modelers with a point of entry for addressing systematic model errors, which would offer hope of improved simulation realism and downstream delivery of more societally relevant model forecasts in the region. An investigation might proceed by evaluating the presence of the error in previous model versions to see if any recent developments have improved (or exacerbated) the issue. Contrasting with the performance of other models may also offer insight. Following this a smaller test case could be identified, such as the forecasts for the particular seasons discussed here. Reforecast experiments could be run to test the impact of changes in model setup, such as resolution, convective parameterization or atmosphere–ocean coupling parameters. Alongside this a close inspection of the day-to-day evolution of the ocean-atmosphere state during particularly extreme errors may provide insight into their origin.

Data Availability Statement

The CHIRPS data (Funk et al., 2015) are available from the Climate Hazards Center at the University of Santa Barbara, USA at https://www.chc.ucsb.edu/data/chirps. The ERA5 data are available from the Copernicus Climate Data Store (Hersbach et al., 2018a; 2018b). This work is based on S2S data. S2S is a joint initiative of the World Weather Research Programme (WWRP) and the World Climate Research Programme (WCRP). The original S2S database (Vitart et al., 2017) is hosted at ECMWF as an extension of the TIGGE database at https://apps.ecmwf.int/datasets/

Acknowledgments
The research was supported by funding from the European Union's Horizon 2020 program through the CONFER (grant 869730) and DOWN2EARTH (grant 869550) projects, from the World Bank funded Accelerating Impacts of CGIAR Climate Research for Africa (grant D7540) project, and from the Research Council of Norway through the Seasonal Forecasting Engine project (grant 270733) and the Climate Futures center (grant 309562). Finally, the authors thank Crameri (2021) for creating the color-vision deficiency friendly and perceptually uniform color maps used here.

References

Bazo, J., Singh, R., Destrooper, M., & Coughlan de Perez, E. (2019). Chapter 18 - Pilot experiences in using seamless forecasts for early action: The "Ready-Set-Go!" approach in the Red Cross. In A. W. Robertson, & F. Vitart (Eds.), *Sub-seasonal to seasonal prediction* (pp. 387–398). Elsevier. https://doi.org/10.1016/b978-0-12-811714-9.00018-8

Behera, S. K., Luo, J.-J., Masson, S., Delecluse, P., Gualdi, S., Navarra, A., & Yamagata, T. (2005). Paramount impact of the Indian Ocean dipole on the East African short rains: A CGCM Study. *Journal of Climate*, *18*(21), 4514–4530. https://doi.org/10.1175/jcli3541.1

Black, E. (2005). The relationship between Indian Ocean sea–surface temperature and East African rainfall. *Philosophical Transactions of the Royal Society A: Mathematical, Physical and Engineering Sciences*, *363*(1826), 43–47. https://doi.org/10.1098/rsta.2004.1474

Black, E., Slingo, J., & Sperber, K. R. (2003). An observational study of the relationship between excessively strong short rains in coastal East Africa and Indian Ocean SST. *Monthly Weather Review*, *131*(1), 74–94. https://doi.org/10.1175/1520-0493(2003)131<0074:AOSOTR>2.0.CO;2

Bruno Soares, M., Daly, M., & Dessai, S. (2018). Assessing the value of seasonal climate forecasts for decision-making. *Wiley Interdisciplinary Reviews: Climate Change*, *9*(4), e523. https://doi.org/10.1002/wcc.523

Conway, D., Allison, E., Felstead, R., & Goulden, M. (2005). Rainfall variability in East Africa: Implications for natural resources management and livelihoods. *Philosophical Transactions of the Royal Society A: Mathematical, Physical and Engineering Sciences*, *363*(1826), 49–54. https://doi.org/10.1098/rsta.2004.1475

Crameri, F. (2021). *Scientific colour maps*. https://doi.org/10.5281/zenodo.4491293

de Andrade, F. M., Young, M. P., MacLeod, D., Hirons, L. C., Woolnough, S. J., & Black, E. (2020). Sub-seasonal precipitation prediction for Africa: Forecast evaluation and sources of predictability. *Weather and Forecasting*, 265–284. https://doi.org/10.1175/waf-d-20-0054.1

Funk, C., Harrison, L., Shukla, S., Pomposi, C., Galu, G., Korecha, D., et al. (2018). Examining the role of unusually warm Indo-Pacific sea-surface temperatures in recent African droughts. *Quarterly Journal of the Royal Meteorological Society*, *144*(S1), 360–383. https://doi.org/10.1002/qj.3266

Funk, C., Peterson, P., Landsfeld, M., Pedreros, D., Verdin, J., Shukla, S., et al. (2015). The climate hazards infrared precipitation with stations—A new environmental record for monitoring extremes. *Scientific Data*, *2*(1), 150066. https://doi.org/10.1038/sdata.2015.66

Haile, G. G., Tang, Q., Sun, S., Huang, Z., Zhang, X., & Liu, X. (2019). Droughts in East Africa: Causes, impacts and resilience. *Earth-Science Reviews*, *193*, 146–161. https://doi.org/10.1016/j.earscirev.2019.04.015

Hansen, J. W., Mason, S. J., Sun, L., & Tall, A. (2011). Review of seasonal climate forecasting for agriculture in Sub-Saharan Africa. *Experimental Agriculture*, *47*(2), 205–240. https://doi.org/10.1017/S0014479710000876
Hastenrath, S. (2007). Circulation mechanisms of climate anomalies in East Africa and the equatorial Indian Ocean. *Dynamics of Atmospheres and Oceans*, *43*(1), 25–35. https://doi.org/10.1016/j.dynatmoce.2006.06.002
Hastenrath, S., Polzin, D., & Camberlin, P. (2004). Exploring the predictability of the 'Short Rains' at the coast of East Africa. *International Journal of Climatology*, *24*(11), 1333–1343. https://doi.org/10.1002/joc.1070
Hersbach, H., Bell, B., Berrisford, P., Biavati, G., Horányi, A., Muñoz Sabater, J., et al. (2018a). *ERA5 hourly data on pressure levels from 1979 to present*. https://doi.org/10.24381/cds.bd0915c6
Hersbach, H., Bell, B., Berrisford, P., Biavati, G., Horányi, A., Muñoz Sabater, J., et al. (2018b). *ERA5 hourly data on single levels from 1979 to present*. https://doi.org/10.24381/cds.adbb2d47
Hersbach, H., Bell, B., Berrisford, P., Hirahara, S., Horányi, A., Muñoz-Sabater, J., et al. (2020). The ERA5 global reanalysis. *Quarterly Journal of the Royal Meteorological Society*, *146*(730), 1999–2049. https://doi.org/10.1002/qj.3803
Hirons, L., & Turner, A. (2018). The impact of Indian Ocean mean-state biases in climate models on the representation of the East African Short Rains. *Journal of Climate*, *31*(16), 6611–6631. https://doi.org/10.1175/jcli-d-17-0804.1
Indeje, M., Semazzi, F. H. M., & Ogallo, L. J. (2000). ENSO signals in East African rainfall seasons. *International Journal of Climatology*, *20*(1), 19–46. https://doi.org/10.1002/(SICI)1097-0088(200001)20:1<19::AID-JOC449>3.0.CO;2-0
Kilavi, M., MacLeod, D., Ambani, M., Robbins, J., Dankers, R., Graham, R., et al. (2018). Extreme rainfall and flooding over central Kenya including Nairobi City during the Long-Rains Season 2018: Causes, predictability, and potential for early warning and actions. *Atmosphere*, *9*(12), 472. https://doi.org/10.3390/atmos9120472
King, J. A., Washington, R., & Engelstaedter, S. (2021). Representation of the Indian Ocean Walker circulation in climate models and links to Kenyan rainfall. *International Journal of Climatology*, *41*(S1), E616–E643. https://doi.org/10.1002/joc.6714
Kolstad, E. W., Wulff, C. O., Domeisen, D. I. V., & Woollings, T. (2020). Tracing North Atlantic oscillation forecast errors to stratospheric origins. *Journal of Climate*, *33*(21), 9145–9157. https://doi.org/10.1175/jcli-d-20-0270.1
Krzywinski, M., & Altman, N. (2014). Visualizing samples with box plots. *Nature Methods*, *11*(2), 119–120. https://doi.org/10.1038/nmeth.2813
Lemos, M. C., Kirchhoff, C. J., & Ramprasad, V. (2012). Narrowing the climate information usability gap. *Nature Climate Change*, *2*(11), 789–794. https://doi.org/10.1038/nclimate1614
Little, P. D., Mahmoud, H., & Coppock, D. L. (2001). When deserts flood: Risk management and climatic processes among East African pastoralists. *Climate Research*, *19*(2), 149–159. https://doi.org/10.3354/cr019149
Liu, W., Cook, K. H., & Vizy, E. K. (2020). Influence of Indian Ocean SST regionality on the East African short rains. *Climate Dynamics*, *54*(11–12), 4991–5011. https://doi.org/10.1007/s00382-020-05265-8
MacLeod, D. (2018). Seasonal predictability of onset and cessation of the east African rains. *Weather and Climate Extremes*, *21*, 27–35. https://doi.org/10.1016/j.wace.2018.05.003
MacLeod, D. A., Dankers, R., Graham, R., Guigma, K., Jenkins, L., Todd, M. C., et al. (2021). Drivers and subseasonal predictability of heavy rainfall in equatorial East Africa and relationship with flood risk. *Journal of Hydrometeorology*, 887–903. https://doi.org/10.1175/jhm-d-20-0211.1
Marchant, R., Mumbi, C., Behera, S., & Yamagata, T. (2007). The Indian Ocean dipole – The unsung driver of climatic variability in East Africa. *African Journal of Ecology*, *45*(1), 4–16. https://doi.org/10.1111/j.1365-2028.2006.00707.x
Matsueda, M., & Palmer, T. N. (2018). Estimates of flow-dependent predictability of wintertime Euro-Atlantic weather regimes in medium-range forecasts. *Quarterly Journal of the Royal Meteorological Society*, *144*(713), 1012–1027. https://doi.org/10.1002/qj.3265
Minami, A., & Takaya, Y. (2020). Enhanced Northern Hemisphere correlation skill of subseasonal predictions in the strong negative phase of the Arctic Oscillation. *Journal of Geophysical Research: Atmospheres*, *125*, e2019JD031268. https://doi.org/10.1029/2019JD031268
Mutai, C. C., & Ward, M. N. (2000). East African rainfall and the Tropical circulation/convection on intraseasonal to interannual timescales. *Journal of Climate*, *13*(22), 3915–3939. https://doi.org/10.1175/1520-0442(2000)013<3915:EARATT>2.0.CO;2
Mutai, C. C., Ward, M. N., & Colman, A. W. (1998). Towards the prediction of the East Africa short rains based on sea-surface temperature–atmosphere coupling. *International Journal of Climatology*, *18*(9), 975–997. https://doi.org/10.1002/(SICI)1097-0088(199807)18:9<975::AID-JOC259>3.0.CO;2-U
Mwangi, E., Wetterhall, F., Dutra, E., Di Giuseppe, F., & Pappenberger, F. (2014). Forecasting droughts in East Africa. *Hydrology and Earth System Sciences*, *18*(2), 611–620. https://doi.org/10.5194/hess-18-611-2014
Nicholson, S. E. (2017). Climate and climatic variability of rainfall over eastern Africa. *Reviews of Geophysics*, *55*, 590–635. https://doi.org/10.1002/2016RG000544
Nyamekye, A. B., Nyadzi, E., Dewulf, A., Werners, S., Van Slobbe, E., Biesbroek, R. G., et al. (2021). Forecast probability, lead time and farmer decision-making in rice farming systems in Northern Ghana. *Climate Risk Management*, *31*, 100258. https://doi.org/10.1016/j.crm.2020.100258
Ogutu, G. E. O., Franssen, W. H. P., Supit, I., Omondi, P., & Hutjes, R. W. A. (2017). Skill of ECMWF system-4 ensemble seasonal climate forecasts for East Africa. *International Journal of Climatology*, *37*(5), 2734–2756. https://doi.org/10.1002/joc.4876
Philippon, N., Camberlin, P., & Fauchereau, N. (2002). Empirical predictability study of October–December East African rainfall. *Quarterly Journal of the Royal Meteorological Society*, *128*(585), 2239–2256. https://doi.org/10.1256/qj.01.190
Robinson, E. S., Yang, X., & Lee, J.-E. (2019). Ecosystem productivity and water stress in Tropical East Africa: A case study of the 2010–2011 drought. *Land*, *8*(3), 52. https://doi.org/10.3390/land8030052
Tall, A., Coulibaly, J. Y., & Diop, M. (2018). Do climate services make a difference? A review of evaluation methodologies and practices to assess the value of climate information services for farmers: Implications for Africa. *Climate Services*, *11*, 1–12. https://doi.org/10.1016/j.cliser.2018.06.001
Ummenhofer, C. C., Sen Gupta, A., England, M. H., & Reason, C. J. C. (2009). Contributions of Indian Ocean Sea surface temperatures to enhanced east African rainfall. *Journal of Climate*, *22*(4), 993–1013. https://doi.org/10.1175/2008jcli2493.1
Vigaud, N., Tippett, M. K., & Robertson, A. W. (2019). Deterministic skill of subseasonal precipitation forecasts for the East Africa-West Asia Sector from September to May. *Journal of Geophysical Research: Atmospheres*, *124*, 11887–11896. https://doi.org/10.1029/2019JD030747
Vitart, F., Ardilouze, C., Bonet, A., Brookshaw, A., Chen, M., Codorean, C., et al. (2017). The Subseasonal to Seasonal (S2S) Prediction Project Database. *Bulletin of the American Meteorological Society*, *98*(1), 163–173. https://doi.org/10.1175/BAMS-D-16-0017.1
Wainwright, C. M., Finney, D. L., Kilavi, M., Black, E., & Marsham, J. H. (2021). Extreme rainfall in East Africa, October 2019–January 2020 and context under future climate change. *Weather*, *76*(1), 26–31. https://doi.org/10.1002/wea.3824

Walker, D. P., Birch, C. E., Marsham, J. H., Scaife, A. A., Graham, R. J., & Segele, Z. T. J. C. D. (2019). *Skill of dynamical and GHACOF consensus seasonal forecasts of East African rainfall*. https://doi.org/10.1007/s00382-019-04835-9

Young, H. R., & Klingaman, N. P. (2020). Skill of seasonal rainfall and temperature forecasts for East Africa. *Weather and Forecasting*, *35*(5), 1783–1800. https://doi.org/10.1175/waf-d-19-0061.1

Zhao, S., & Cook, K. H. (2021). Influence of Walker circulations on East African rainfall. *Climate Dynamics*, *56*. https://doi.org/10.1007/s00382-020-05579-7